JOURNAL OF GEOPHYSICAL RESEARCH, VOL. 104, NO. B8, PAGES 17,879–17,896, AUGUST 10, 1999

Streaming potential measurements 2. Relationship between electrical and hydraulic flow patterns from rock samples during deformation

Benoit Lorne, Frédéric Perrier, and Jean-Philippe Avouac

Commissariat à l'Énergie Atomique, Laboratoire de Détection et de Géophysique, Bruyères-le-Châtel, France

Abstract. Streaming potential and resistivity measurements have been performed on Fontainebleau sandstone and Villejust quartzite samples in a triaxial device during compaction, uniaxial compression, and rupture. Measurements on individual samples do not show any clear intrinsic dependence of the streaming potential coefficient with permeability. An apparent dependence of the streaming potential coefficient with permeability is, however, observed during deformation. The effect of surface conductivity is taken into account and is small compared with the observed changes in the streaming potential coefficient. The observed dependence is therefore interpreted in terms of a difference in the evolution of the electrical and hydraulic connectivity patterns during deformation. This effect causes the streaming potential coefficient, and consequently the inferred ζ potential, to be reduced by a geometrical factor R_G representing the electrical efficiency of the hydraulic network. Estimates of the R_G factor varying between 0.2 and 0.8 for electrolyte resistivity larger than 100 Ωm are obtained by comparing the values of the ζ potential inferred from intact rock samples with the values obtained from crushed rock samples, where the geometrical effects are assumed to be negligible. The reduction of the streaming potential coefficient observed during compaction or uniaxial compression suggests that the tortuosity of the hydraulic network increases faster than the tortuosity of the electrical network. Before rupture, an increase in the streaming potential coefficient associated with the onset of dilatancy was observed for three samples of Fontainebleau sandstone and one sample of Villejust quartzite. The changes in streaming potential coefficient prior to failure range from 30% to 50%. During one experiment, an increase in the concentration of sulfate ions was also observed before failure. These experiments suggest that observable streaming potential and geochemical variations could occur before earthquakes.

1. Introduction

This paper is the second part of a study devoted to an experimental investigation of the electrokinetic effect (EKE) in the laboratory. As discussed at length by *Lorne et al*. [this issue], this study is motivated by the fact that variations of electric potential observed in a variety of geophysical contexts (geothermal fields, volcanoes, and, in some instances, before earthquakes) remain poorly understood. In the companion paper we used crushed samples to investigate the properties of the electrical double layer (EDL), which is at the core of the EKE, and some empirical laws were obtained. To assess the EKE in natural systems, in the present study we investigate the relationship between fluid flow and electric potentials during deformation and rupture. The streaming potential coefficient, which is the ratio of the electric potential to the pressure gradient, is measured by recording the voltage across a sample through which an electrolyte is flowing. The streaming potential coefficient (also called the electrokinetic coupling coefficient) is proportional to the pressure gradient and a quantity called the ζ potential, which characterizes the structure of the EDL.

Paper number 1999JB900155.
0148-0227/99/1999JB900155$09.00

Earlier measurements of the streaming potential coefficient with rock samples were performed by *Jouniaux and Pozzi* [1995a, b, 1997] in a triaxial device, and the effect of deformation and rupture was studied. The reported values of the ζ potential for Fontainebleau sandstone and a 1 mmol/L 1:1 electrolyte solution at pH = 5.6 varied from −20 to −97 mV.

In this paper we first compare ζ potentials inferred from streaming potential measurements of crushed Fontainebleau sandstone samples, reported by *Lorne et al*. [this issue], with results using intact rock samples. This systematic comparison between crushed and intact rock samples is also of potential value for rock formations for which the sample permeability in the laboratory is small, whereas the permeability in the field is high because of a pattern of fractures at large scales. For such rock formations one could measure the ζ potential of crushed samples and extrapolate to the field scale using the scaling relations empirically established for Fontainebleau sandstone.

When extrapolating to the large scale, the question of the permeability dependence of the streaming potential coefficient arises. The effect of permeability was addressed by *Jouniaux and Pozzi* [1995a] using Fontainebleau sandstone and Mériel limestone samples. They found a permeability dependence of the streaming potential coefficient, which they interpreted to result from the variation of surface conductivity with permeability. However, we question this interpretation since, first, it relies on a value of the surface conductance of Fontainebleau

sandstone of $5 \times 10^{-9}\ \Omega^{-1}$, which corresponds to values of surface conductivity as large as 3.4 mS/m, a value which is incompatible with the value 0.07 mS/m measured experimentally [*Ruffet et al.*, 1991]; and, second, the Kozeny-Carman model [*Scheidegger*, 1974] is used to predict that surface conductivity approximately scales as $k^{-0.5}$, where k is the permeability. For a change in permeability from 10^{-16} to 10^{-12} m^2, as considered by *Jouniaux and Pozzi* [1995a], the surface conductivity should increase by about a factor of 100. No experimental evidence for such a large effect has been reported so far. The interpretation by *Jouniaux and Pozzi* [1995a] may therefore have overestimated the role played by the surface conductivity. It appears crucial therefore to measure the streaming potential coefficient and the surface conductivity simultaneously as a function of permeability.

Studying the permeability dependence of the streaming potential coefficient also raises fundamental questions in rock physics. Until now, the interpretations of the streaming potential results in rocks have been based on the Helmholtz-Smoluchowski equation [*Overbeek*, 1960] derived for capillary tubes. This equation relates the streaming potential coefficient to the ζ potential and predicts that the streaming potential coefficient has no intrinsic dependence on permeability, once surface conductivity effects are taken into account. In the context of porous media, *Pride* [1994] showed that the Helmholtz-Smoluchowski equation was also valid when a statistical volume averaging procedure is used. However, this relation needs to be tested experimentally, and this is the purpose of this paper.

2. Streaming Potentials in Rocks

The conductivity (resistivity) of the rock sample is noted σ_r (ρ_r), while the conductivity (resistivity) of the electrolyte saturating the pore space is noted σ_f (ρ_f). The rock conductivity can be expressed as

$$\sigma_r = \frac{\sigma_f}{F} = \frac{\sigma_f}{F_0} + \sigma_s, \tag{1}$$

where F is called the formation factor, F_0 is the bulk formation factor, and the constant σ_s is the surface conductivity.

2.1. EKE in Capillary Models

In the equivalent channel model of Kozeny and Carman [*Scheidegger*, 1974] the pore space of the rock sample is represented by a capillary tube of section S_c and length L_c in a typical volume of electrically insulating material of length L and section S (Figure 1a). The ratio L_c/L is known as the hydraulic tortuosity τ.

In this model the bulk formation factor F_0 can be written as

$$1/F_0 = \Phi/\tau^2, \tag{2}$$

where Φ is the volume fraction of the pore space (porosity), and the surface conductivity σ_S as [*Ishido and Mizutani*, 1981]

$$\sigma_s = k_s \frac{S_i}{\tau^2}, \tag{3}$$

where k_s is the surface conductance of the capillary and S_i is its specific internal area (internal pore surface area per volume of rock sample).

The permeability k is given by

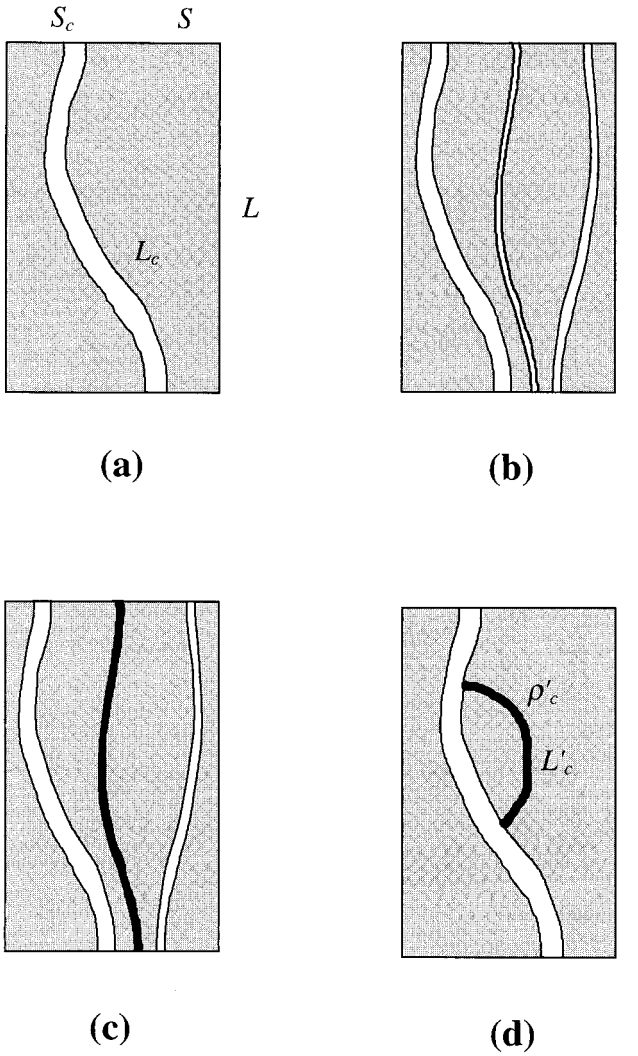

Figure 1. Various flow patterns in capillary tubes in a nonconducting matrix: (a) one single capillary (equivalent channel), (b) distribution of capillary tubes of various diameters and tortuosities, (c) distribution of capillaries including some containing a nonflowing conducting medium (in black), and (d) capillary tube with a branch containing a nonflowing conducting medium.

$$k = c \frac{\Phi^3}{S_i^2 \tau^2}, \tag{4}$$

where c is a constant depending on the geometry of the capillary; $c = 0.5$ for tubes and 1/3 for cracks [*Scheidegger*, 1974].

If a pressure difference Δp is applied to the rock sample, the resulting motion of the electrolyte results in an electrical convection current I_{conv}:

$$I_{\text{conv}} = -\frac{\varepsilon}{\eta} \zeta \frac{S}{F_0} \frac{\Delta p}{L}, \tag{5}$$

where η is the dynamic viscosity of the electrolyte, ε is its electrical permittivity [*Overbeek*, 1960; *Ishido and Mizutani*, 1981], and ζ is the electrical potential on the shear plane [*Bikerman*, 1964; *Lorne et al.*, this issue].

Let ΔV be the potential difference between the two ends of the rock sample, taking the reference point for potential at the high pressure end, following *Morgan et al.* [1989]. If R is the

electrical resistance of the rock sample, the conduction current I_{cond} is

$$I_{\text{cond}} = \Delta V/R. \tag{6}$$

If the rock sample is electrically isolated, the conduction and the convection currents are equal and the streaming potential coefficient C_s, defined by $C_s = \Delta V/\Delta p$, is given by the Helmholtz-Smoluchowski equation [*Overbeek*, 1960; *Ishido and Mizutani*, 1981; *Pride*, 1994; *Revil et al*., 1996]

$$C_s = \frac{\Delta V}{\Delta p} = -\frac{\varepsilon}{\eta}\,\zeta\rho_f G. \tag{7}$$

with (equations (5) and (6))

$$G = F/F_0. \tag{8}$$

This relationship remains valid if the rock is modeled by a distribution of independent capillaries of various sizes (Figure 1b) and if some of these capillaries are electrically conducting but nonflowing (Figure 1c). More generally, (8) has also been shown to hold in the context of a pore space volume averaging procedure [*Pride*, 1994]. However, some situations where this relation may not be valid are discussed in section 2.2.

2.2. Effect of Independent Hydraulic and Electrical Networks

Imagine that the patterns of electrical and hydraulic pathways do not coincide. On the one hand, all the pores contributing to the permeability must contribute to the electrical conductivity. On the other hand, very tiny pores or conducting mineral phases, like sulfides or carbon, may contribute to the electrical connectivity although they may not participate in the hydraulic network.

Consider, for example, the hypothetical rock sample depicted in Figure 1d. It has a capillary tube with a branch of a noncirculating conductive phase of length L_c'. If the surface conductivity is neglected, one has $F/F_0 = 1$. However, in such a model, assuming that the conductance of the branching channel is much larger than the conductance of the channel with electrolyte, the electrical path is reduced compared with the hydraulic path by a factor L_c'/L_c, and one has

$$G \approx \frac{L_c - L_c'}{L_c}, \tag{9}$$

and (8) is violated.

This example of a different percolation path for the hydraulic and electrical flows may not be a purely theoretical case. In a real rock, there are always several interconnected percolation networks and at least a bulk pore space conductivity and a grain surface conductivity. Surface roughness can also create locally different directions for fluid flow and the electric current in a single fracture or joints [*Brown*, 1987, 1989; *Walsch et al*., 1997; *Glover et al*., 1997a].

To describe this effect, *David* [1993] introduced the concept of hydraulic and electrical tortuosities τ_h and τ_e, defined in the context of the equivalent channel model of Kozeny-Carman by

$$\begin{aligned} 1/F_0 &= \Phi/\tau_e^2 \\ k &= c\,\frac{\Phi^3}{S_i^2\tau_h^2}. \end{aligned} \tag{10}$$

On the basis of a reasonable number of network calculations, *David* [1993] found that the hydraulic tortuosity is larger than the electrical tortuosity by a factor of 1.5. In this context, the convection current (equation (5)) would scale like $1/\tau_h$, the resistance would scale like $1/\tau_e$, and one would expect a relationship of the type

$$G \approx \tau_e/\tau_h. \tag{11}$$

Let us consider the quantity defined by

$$R_G = G\,\frac{F_0}{F}. \tag{12}$$

This quantity R_G is expected to be related to the electrical efficiency of the hydraulic network and should be <1. By contrast, the factor F/F_0 expresses the hydraulic efficiency of the electrical network. Our approach in this paper is to obtain some estimates of R_G from measurements of the streaming potential and the resistivity for intact rock samples.

In the following, the streaming potential coefficient will be corrected from surface conductivity effects using an experimentally measured value of the ratio F/F_0:

$$\frac{F}{F_0} = \frac{\rho_0}{\rho_f}\,\frac{R(\rho_f)}{R(\rho_0)}, \tag{13}$$

where ρ_0 is a value of the electrolyte resistivity for which the electrolyte bulk conductivity dominates the sample conductivity.

Correcting the streaming potential coefficient for surface conductivity effects using the ratio F/F_0 obtained from (13), the inferred ζ potential, called the effective potential and noted ζ_{eff}, is

$$\zeta_{\text{eff}} = -14\,\frac{C_s}{\rho_f}\,\frac{F_0}{F}, \tag{14}$$

with C_s expressed in mV/0.1 MPa, ζ in mV, and ρ_f in Ωm. A value of 7×10^{-10} F/m has been assumed for the water permittivity, and a value of 10^{-3} Pa s has been assumed for the water viscosity at 25°C.

Using the definition of the R_G factor (11), the effective ζ potential is related to the true ζ potential by the relationship

$$\zeta_{\text{eff}}(\rho_f,\ \text{rock}) = R_G(\rho_f,\ \text{rock})\,\zeta(\rho_f,\ \text{minerals}). \tag{15}$$

The parameter R_G in general depends both on the rock and the electrolyte properties. The true ζ potential depends only on the properties of the mineral-electrolyte interface because the effect of the pore size on the ζ potential is negligible [*Pride and Morgan*, 1991; *Pride*, 1994; *Lorne et al*., this issue, appendix]. In crushed samples, which are far above the percolation thresholds, the effects due to differences in the electrical and hydraulic flows will be assumed to be negligible, and therefore the measured ζ potential with crushed samples provides the true ζ potential.

3. Experimental Setup

3.1. Sample Assembly and Triaxial Cell

The triaxial cell is shown in Figure 2, and an overview of the experimental setup is shown in Figure 3. Stainless steel 5 mm thick electrodes are placed at both ends of the rock sample, which has a diameter of 36 or 30 mm and a length of 72 mm. A sheet of tissue (Rilsan) is inserted between the electrode and the rock sample to ensure a good electrical contact between the rock sample and the electrode (M. Darot, personal com-

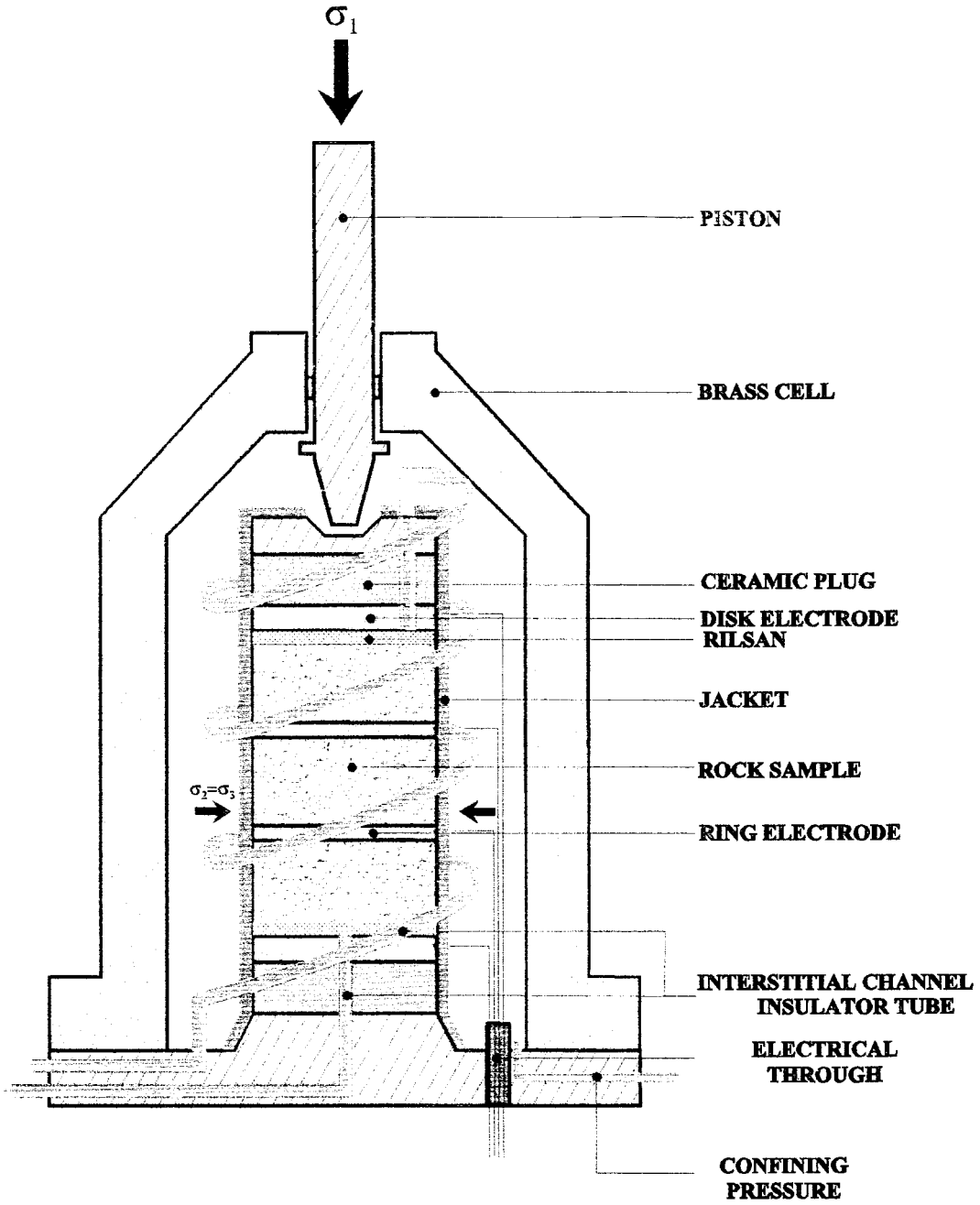

Figure 2. The triaxial cell used for streaming potential and resistivity measurements using rock samples.

munication, 1994). Ceramic plugs with a thickness of 5 mm are inserted between the stainless steel base of the cell and the bottom electrode, and the stainless steel cap and the upper electrode. A polymer jacket (Rhodorsil) is formed around the sample assembly in a polymer mold, which is then removed. In addition, a heat shrinkable sleeve encases the ceramic plug and the electrode as well as the top 1 cm of the rock in order to avoid fluid circulation between the sample and the jacket. Contact areas between the jacket and the tubes are sealed by silicon glue.

The interstitial fluid is circulated out of the sample through 1.2 m long stainless steel tubing. In order to prevent any contact between the interstitial fluid and the metal pieces of the assembly, a Teflon tube with an inner diameter of 0.81 mm and a outer diameter of 1.63 mm is inserted in the stainless steel flow channel (Figure 2). This polymer tubing reaches to the rock sample through the ceramic plug and the electrode. It can be used up to internal pressures of 18 MPa. Another slightly larger tube was similarly inserted in the inlet flow channel. In order to prevent collapse of the small tubes under pressure, a syringe needle is inserted in the end of the tubes near the electrode, at the contact point with the Rilsan. The polymer tube suppresses any leakage resistance parallel to the rock sample and also protects the electrolyte from chemical contamination by the brass metal pieces.

A confining pressure is applied in the brass cell around the

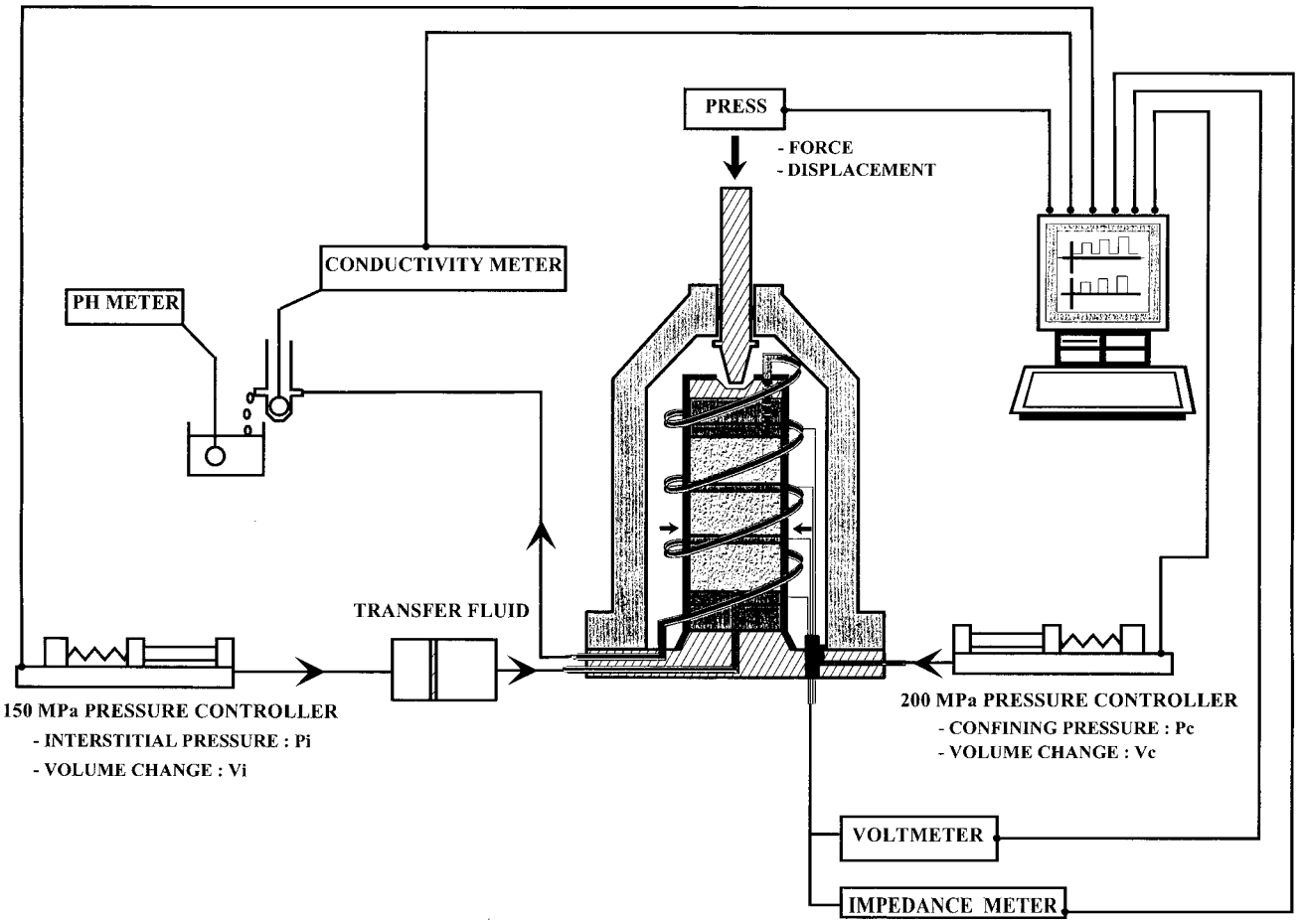

Figure 3. The experimental setup used for streaming potential and resistivity measurements using rock samples.

sample through a degassed distilled water circuit connected to an external pressure controller which has a maximum range of 200 MPa (Figure 3). The interstitial fluid is contained in a transfer cell (volume 180 mL) connected to an external pressure controller of 150 MPa maximum range. The electrolyte is circulated from the bottom to the top of the sample, but the direction of the flow can be reversed if needed. The electrolyte that has circulated in the rock sample is collected after flowing through a conductivity cell for pH measurement for chemical analysis. The maximum flow rate possible for the interstitial fluid is 6 mL/min. The pressure generators provide a precision of 1 mm^3 on the volumes. The precision of these generators for measuring pressure is, however, not adequate for all experiments, and a pressure transducer having an accuracy of 0.35 kPa and a maximum pressure of 250 kPa is connected to the entrance of the interstitial fluid loop. The maximum interstitial pressure used during the experiments was 200 kPa for most samples. For some samples a maximum pressure of 1.5 MPa was used, and for this pressure range the pressure measurement from the pressure generator transducer was used.

Uniaxial force is applied from the top by a press held by two columns whose rigidity is $>10^{11}$ Pa. The maximum force is 100 kN, corresponding to a pressure of 98 MPa for a 36 mm diameter sample and 140 MPa for a 30 mm diameter sample. The press can be servocontrolled in force or displacement.

The pressure, conductivity, pH, and electrical measurement devices are described by *Lorne et al*. [this issue]. Flow rates, pressures, force, displacement, conductivity, and electrical measurements are recorded with a sampling time of 1 s.

3.2. Permeability Measurements

The permeability is computed from the volume flow given by the pressure generators (accuracy of ± 1 mm^3) and the pressure gradient, taking into account the head loss in the circuit. The head loss is dominated by the pressure gradient along the small polymer tubing at the outlet and amounts to 10 kPa for a flow rate of 6 mL/min. The calculated value was experimentally checked without any rock sample in the cell. The smallest measured permeability in the experiment was 0.1 mdarcy (10^{-16} m^2). Most samples used for the measurements in this paper had a permeability larger than 10 mdarcy (10^{-14} m^2).

3.3. Chemical Measurements

The electrolytes were prepared as by *Lorne et al*. [this issue] using KCl as a salt, with a pH of 5.7. The solutions flowing out of the samples were sampled during some experiments in order to check for contamination of the electrolyte by the rock and to monitor chemical changes during deformation. The dominant ion content of the samples was determined by electrophoresis.

3.4. Electrical Measurements

The stainless steel electrodes were stable enough to measure the streaming potentials down to values of order 1 mV [see

Table 1. Main Characteristics of the Rock Samples

	Φ, %	k, mdarcy	F_0	σ_S, mS/m	Experiment
Fontainebleau sandstone					
FS1	16.0	340	21.8	0.01 ± 0.003	C
FS2	17.5	36	53.0	0.03 ± 0.008	C
FS3		210	34.1	0.05 ± 0.008	C
FS4		64			R
FS5		83	48.5	0.06 ± 0.006	C + R
FS6		140	22.3	0.04 ± 0.007	R
Villejust quartzite					
VQ1	3.4	11.5	223.5	0.01 ± 0.004	C
VQ2	6–8	2.5			R
VQ3	6–8	8.9	123.0		R
Vosges sandstone					
VS1		6.8	12.5	2 ± 0.7	
Alps rocks					
AS1		0.013			
AD1		0.15			

For each sample, the initial porosity (Φ), permeability (k), bulk formation factor (F_0), and surface conductivity (σ_S) are given. C stands for compaction experiment, and R stands for rupture. The porosity was measured by mercury injection (see text).

Lorne et al., this issue]. The quality of the stainless steel was found, however, to be a critical factor for stability, and SS316L steel was used, as in marine applications. Poorer quality steels, brass, or copper showed corrosion after dismantling and were unstable. Platinum electrodes provide good electrical contacts for resistivity measurements [*Lockner and Byerlee*, 1985; *Ruffet et al*., 1991; *Glover et al*., 1994], but the measurement of streaming potentials using platinum electrodes can be affected by large motoelectrical potentials [*Ogilvy et al*., 1969] depending on the electrode arrangement and the setup. Silver electrodes [*Morgan et al*., 1989] could not be used in our pressure cell.

In contrast to the setup used by *Jouniaux and Pozzi* [1995b], the small tubes inserted in the interstitial flow channels prevented leakage resistance in parallel with the rock sample. The small tube also prevented electrolyte leakage into the confining pressure reservoir, which would also produce leakage resistance. The potential measurements were extremely stable with this setup (measured drift of the order of 1 mV/h or smaller), and no difference was seen in the DC value of the electric potential if one of the electrodes was connected to either the ground of the cell or the ground of other measuring devices.

3.5. Rock Samples and Experimental Protocol

The main characteristics of the rock samples used for the experiments presented in this paper are listed in Table 1. Most measurements were performed using prediagenetic Fontainebleau sandstone, for which most experimental data exist. We also made measurements on other types of rocks. The porosity was determined by mercury injection in samples drilled from the same block of rock used to obtain samples for streaming potential measurements, since after mercury injection, electrical measurements could not be made. Thus porosity of the samples is not measured for the same samples as those used for electrical measurements, except for samples FS1 and FS2 after compaction, whose porosity was measured after all streaming potential measurements were completed.

The Fontainebleau sandstone contains >99% quartz with traces of calcareous cement, with an average grain size of 125 μm. The Villejust quartzite contains >99.5% quartz, with an average grain size of 200 μm. The grains of the quartzite are rounded, closely imbricated, producing a small porosity (5–8%) and a permeability near the percolation threshold [e.g., *Duplessis and Roos*, 1994; *Knackstedt and Duplessis*, 1996]. The Vosges sandstone contains a mass fraction of 3–4% of oxides and ~11% clay [*David et al*., 1994]. We also measured a sample of calcareous Permian sandstone (AS1) and a sample of cellular dolomite (AD1) collected at a geological contact in the Alps [*Perrier et al*., 1998; *Trique et al*., 1999].

After installation in the triaxial cell the sample is cleaned by circulating degassed pure water with a conductivity varying between 5×10^3 and 10^4 Ωm (depending on impurities leached from the rock) for >1 day. Next, the electrolyte is circulated through the sample, and the conductivity is monitored at the outlet. After a stabilization time which depends on the sample permeability, the output conductivity as well as the rock resistance become stable.

The streaming potential ΔV is then measured for several pressure gradients Δp. A typical streaming potential experiment is shown in Figure 4. A stable value of electrical potential is reached a few minutes after the pressure gradient is established. The measured equilibrium potential is corrected for electrode drift assuming a linear variation during the time the electrolyte is flowing and is plotted in Figure 5 as a function of the pressure gradient corrected for head loss. The potential is linearly proportional to the pressure, and the streaming potential coefficient C_s is the slope of this curve. During most experiments, pressure gradients <30 kPa were used to avoid changing the stress state of the rock, and the experimental uncertainty on the streaming potential coefficient varied from 30% for a streaming potential coefficient of 40 mV/0.1 MPa to 2% for a streaming potential coefficient of 1000 mV/0.1 MPa.

Possible edge effects on the sample were estimated by comparing the potential differences measured between various positions along the sample. For this purpose, some experiments were performed with some additional electrodes made of stainless steel rings wrapped around the rock cylinder. The results of one of these experiments are shown in Figure 6, where the potential difference between one disk electrode and one ring electrode near the center of the sample is compared with the symmetric combination on the other side of the sample. The measurements on both sides of the sample are in agreement, with a standard deviation of 7.5 mV for an average value of 75 mV. Therefore the potential is homogeneous

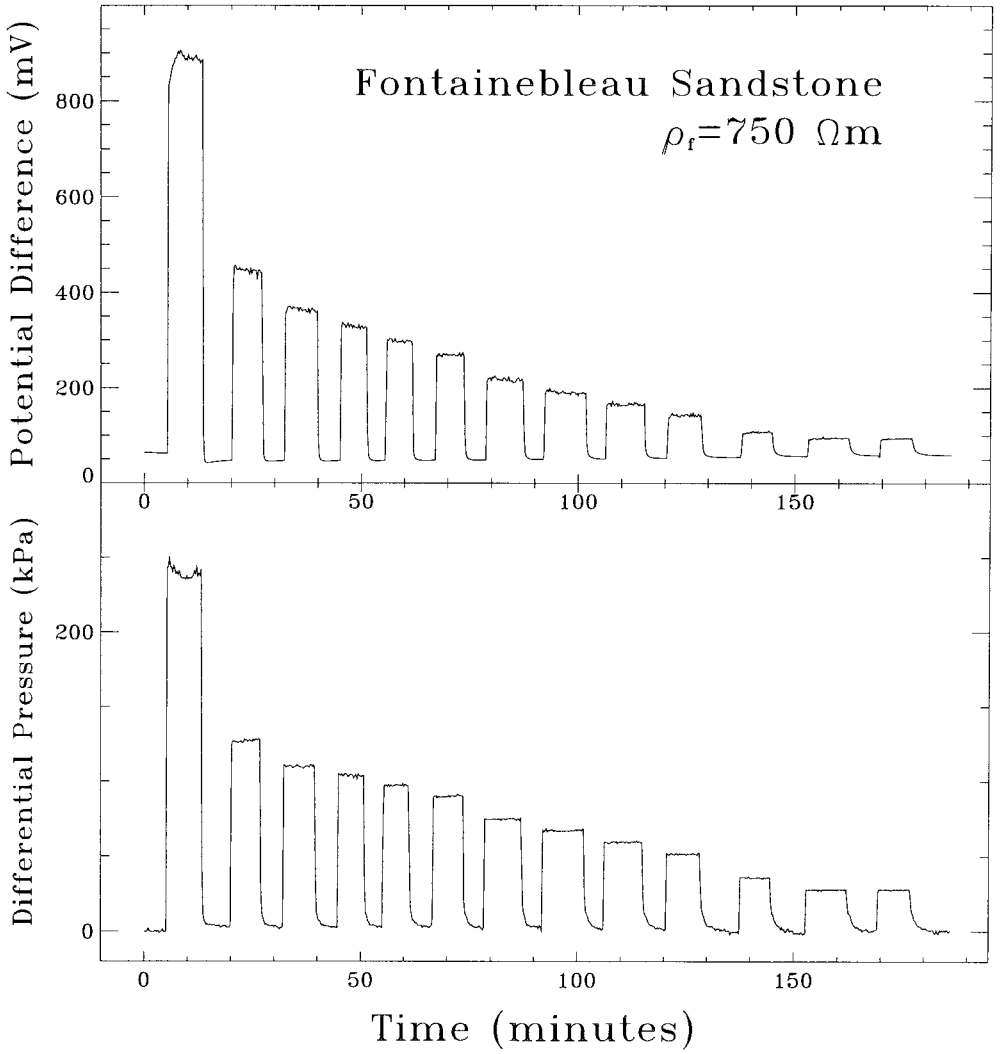

Figure 4. A typical streaming potential measurement with Fontainebleau sandstone. The electric potential reference is taken at the high-pressure end (convention of *Morgan et al*. [1989]). A positive potential difference (i.e., a positive streaming potential coefficient) corresponds to a negative ζ potential. A single measurement of streaming potential takes <10 min to reach a stable value. The electrode drift during that time is in general <1 mV.

within 10% along the sample. This conclusion, however, can not be generalized for any rock sample. Some samples may be more heterogeneous, especially rocks from the Alps containing veins of quartz or calcite, and this may explain most of the variations observed from sample to sample. When measurements were repeated on the same sample after several days, the values of the streaming potential coefficient were reproducible within a few percent if the permeability had not changed.

The formation factor was computed from the measured resistance of the rock sample at 1 kHz, and the bulk formation factor and surface conductivity were determined using (1). Results are shown in Figure 7 for the Vosges sandstone (VS1) and one sample of Fontainebleau sandstone (FS1) after compaction. Values for surface conductivity found in this experiment are in good agreement with the measurements of *Ruffet et al*. [1991] for Vosges sandstone. For Fontainebleau sandstone our results range from 0.01 to 0.06 mS/m (Table 1), whereas *Ruffet et al*. [1991] obtained slightly larger values from 0.07 to 0.09 mS/m. Values as large as 0.5 to 0.7 mS/m have been measured for some samples of Fontainebleau sandstone (P. Glover, private communication, 1997). Such large values tend to be typical of sandstones such as Berea or Darley Dale sandstone containing significant proportions of clays [*Glover et al*., 1994].

In the Kozeny-Carman model, combining (2), (3), and (4), one can write

$$\sigma_s = k_s \frac{\sqrt{c}}{\sqrt{k}\, F_0^{3/2}}. \tag{16}$$

Our estimates of the surface conductivity in Fontainebleau sandstone, listed in Table 1, do not support this simple prediction, used by *Jouniaux and Pozzi* [1995a]. For example, according to (16), sample FS2 should have a surface conductivity reduced by a factor 0.8 compared with sample FS1, but the experimental value for FS2 is 3 times larger than the value for FS1. Similarly, (16) predicts that sample FS6 should have a

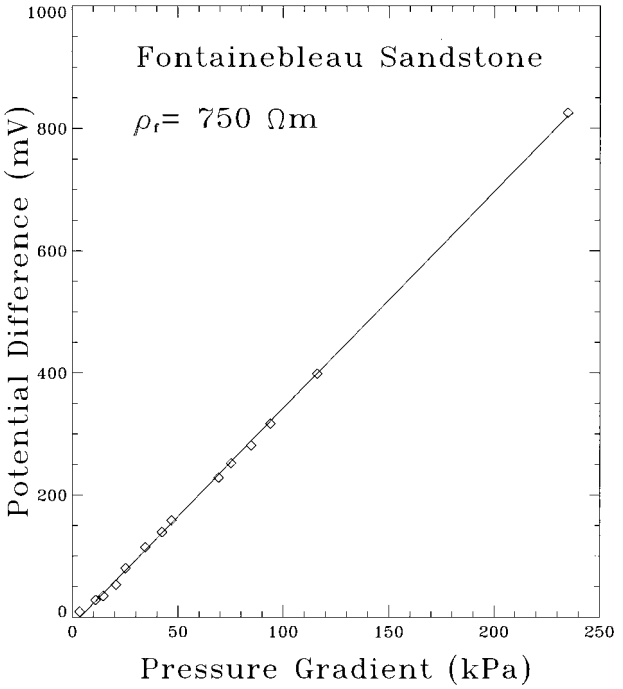

Figure 5. Potential difference as a function of the pressure gradient for the experiment shown in Figure 4. The experimental errors are of the order of the size of the symbols. This experiment yields a positive streaming potential coefficient of 350 mV/0.1 MPa.

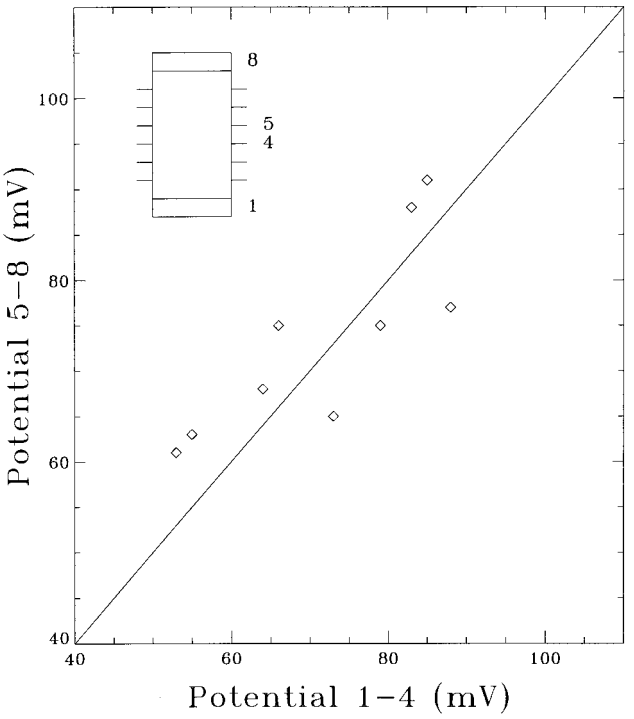

Figure 6. The potential difference between disk electrode 1 and ring electrode 4 compared with the potential difference between ring electrode 5 and disk electrode 8. The position of the electrodes is shown. The various measurements corresponds to several steps during the uniaxial deformation of the sample.

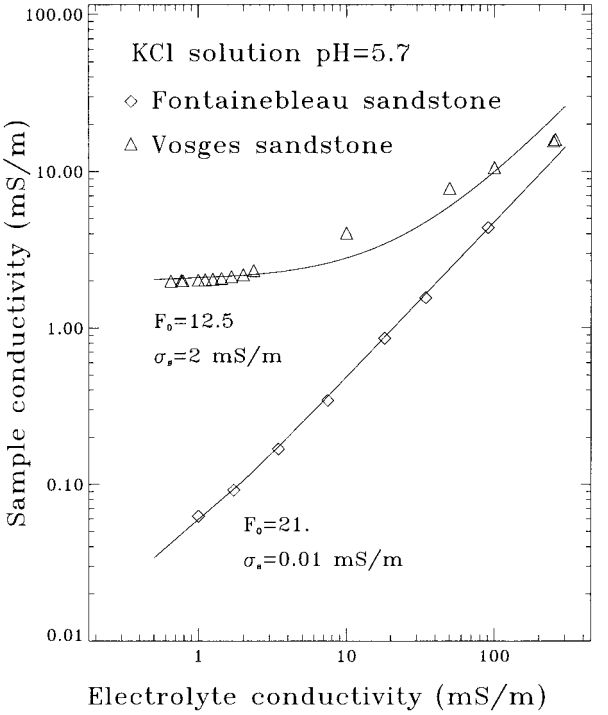

Figure 7. The conductivity of the rock sample versus the conductivity of the KCl solution, for a sample of Fontainebleau sandstone (FS1, compacted) and a sample of Vosges sandstone (VS1). The curve for Fontainebleau sandstone corresponds to a least squares adjustment of equation (6) to the data. The curve for the Vosges sandstone corresponds to the values for the bulk formation factor and the surface conductivity given by *Ruffet et al.* [1991], illustrating the good agreement of the resistivity data of the present experiment with the results of *Ruffet et al.* [1991]. The experimental errors (not including poorly known sample to sample variations) are of the order of the size of the symbols.

surface conductivity 40% larger than sample FS1, but the measured value for FS6 is 4 times larger than the value for FS1. This indicates the importance of other factors determining the surface conductivity (i.e., the proportion of clay impurities or the presence of particularly calcareous surface coatings). Therefore it is preferable, as discussed in section 2.2, not to rely on the Kozeny-Carman model but to measure the ratio F/F_0 to correct the streaming potential coefficient for surface conductivity.

In Figure 8 the F/F_0 factor determined using (13) is shown for one sample of Fontainebleau sandstone as a function of the electrolyte resistivity. For this sample this factor is >0.9 (i.e., a surface conductivity correction of $C_s < 10\%$) for electrolyte resistivity <600 Ωm.

4. Experimental Results Without Deformation and Discussion

4.1. Comparison With Crushed Samples and Effect or Electrolyte Resistivity

The effective ζ potentials, inferred from streaming potential measurements using (14), are presented as a function of electrolyte resistivity in Figure 9 for Fontainebleau sandstone and in Figure 10 for Villejust quartzite.

For Fontainebleau sandstone the values for the ζ_{eff} potential

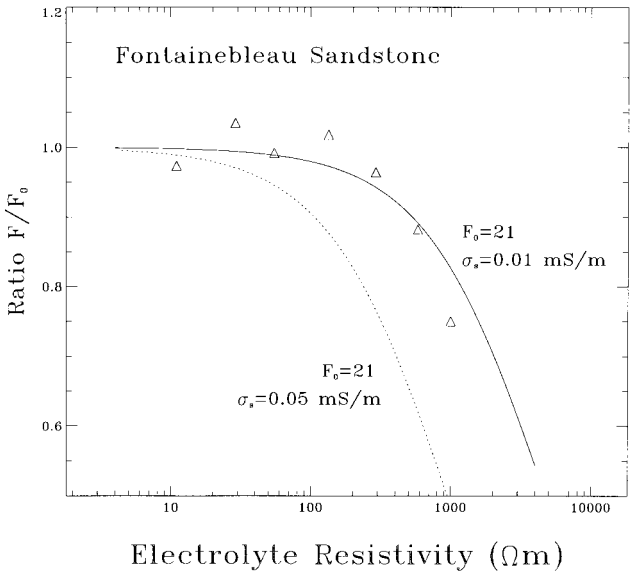

Figure 8. The streaming potential correction factor F/F_0, as derived from the measurements of rock and electrolyte conductivity measurements for one sample of Fontainebleau sandstone (Figure 7). The full line corresponds to the calculated value assuming a bulk formation factor of 21 and a surface conductivity of 0.01 mS/m. The dotted line corresponds to the calculated value assuming a bulk formation factor of 21 and a surface conductivity of 0.05 mS/m.

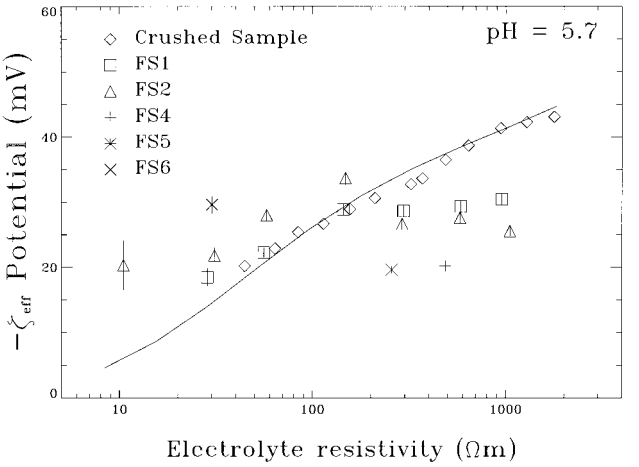

Figure 9. The effective ζ potential, inferred from streaming potential measurements using Fontainebleau sandstone rock samples, as a function of the KCl solution resistivity. The data are compared with measurements obtained for crushed samples [*Lorne et al*., this issue]. The curve corresponds to a theoretical prediction for the quartz-KCl interface obtained with a three-layer numerical model of the electrical double layer [*Lorne et al*., this issue], based on the work of *Davis et al*. [1978]. When not indicated, the experimental errors are given by the size of the symbols.

varies between −20 and −30 mV (Figure 9). For values of the electrolyte resistivity ≲200 Ωm the ζ_{eff} potentials measured for rocks are compatible with those from crushed samples [*Lorne et al*., this issue]. The variation with electrolyte resistivity predicted by the three-layer model based on the work of *Davis et al*. [1978] is also valid for the rock samples. For electrolyte resistivities >200 Ωm the ζ potentials measured for rocks are systematically smaller than those for crushed samples, and the discrepancy increases with increasing electrolyte resistivity.

The Fontainebleau samples used in this experiment are poorly cemented and easily disaggregated without producing fresh crack surfaces in the quartz grains of the rocks. The surface properties of the disaggregated grains are therefore likely to be similar to the surface properties of the grains in the intact rock sample. In addition, the ζ potential measured with the crushed sample was changed by <10% by an acidic treatment [*Lorne et al*., this issue]. Furthermore, any difference in the ζ potential due to differences in surface state between disaggregated and intact samples should also be observed at the lower values of the electrolyte resistivity. As this is not the case (Figure 9), we conclude that the comparison between rock samples and crushed samples may be used to infer a value of the R_G factor ($R_G = \zeta_{\text{eff}}/\zeta_{\text{crushed}}$) ~ 0.5 at 1000 Ω m.

The value of the F/F_0 correction factor calculated via (13) varies from unity at 30 Ωm to 0.9 at 600 Ωm and 0.75 at 1000 Ωm (Figure 8) for sample FS1. The measurement of large rock resistivity can be problematic, but it would probably lead to an underestimation of the resistance, hence an overestimate of the surface conductivity, and, consequently, an underestimate of the F/F_0 factor. However, the F/F_0 factor needed to match the ζ potential values for crushed and rocks samples is smaller than that measured. If the calculation of the F/F_0 factor using (13) is correct, then there must be another physical origin for the R_G factor for electrolyte resistivities >200 Ωm.

The results in Figure 9 agree with the previously reported values for ζ potential of Fontainebleau sandstone of −21.9 mV [*Jouniaux and Pozzi*, 1995b] and −17 mV [*Jouniaux and Pozzi*, 1997]. However, the value of −97 mV mentioned by *Jouniaux and Pozzi* [1995a] is not compatible with our data. This value may have been overestimated because the electrolyte resistivity

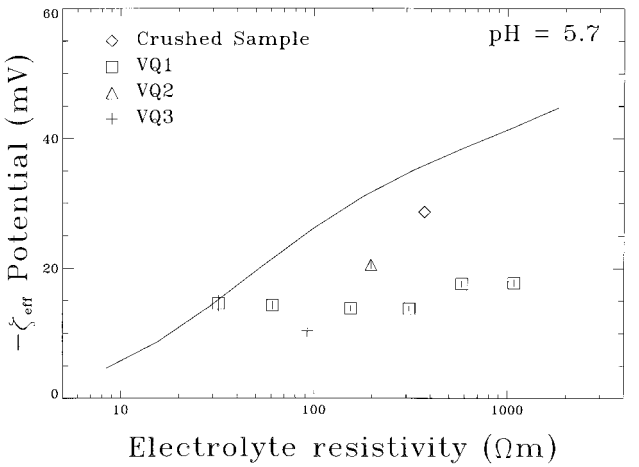

Figure 10. The effective ζ potential, inferred from streaming potential measurements using Villejust quartzite rock samples, as a function of the KCl solution resistivity. The data are compared with one measurement obtained for a crushed sample [*Lorne et al*., this issue]. The curve corresponds to a theoretical prediction for the quartz-KCl interface obtained with a three-layer numerical model of the electrical double layer [*Lorne et al*., this issue], based on the work of *Davis et al*. [1978]. When not indicated, the experimental errors are given by the size of the symbols.

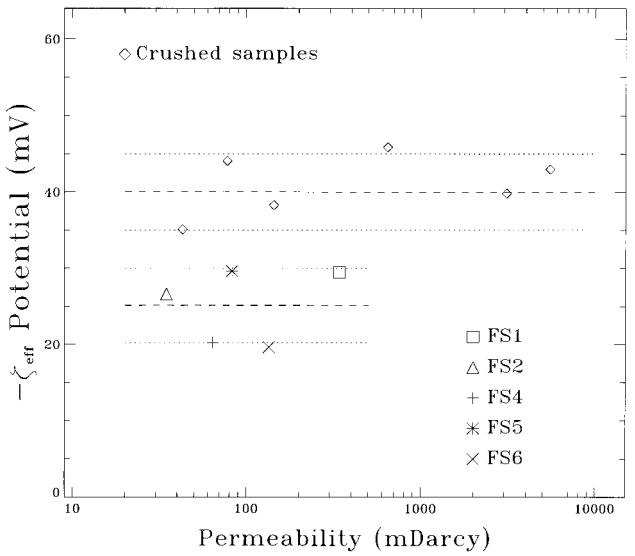

Figure 11. The effective ζ potential, inferred from streaming potential measurements using Fontainebleau sandstone rock samples, as a function of permeability for a KCl solution of 400 Ωm resistivity and pH = 5.7. The data are compared with measurements obtained for crushed samples [*Lorne et al*., this issue]. The error on each individual measurement is given approximately by the size of the symbols. The indicated bands (dotted lines) around the average values (dashed line) indicate a one standard deviation error reflecting sample to sample variations.

was measured as 1000 Ωm at the output of the sample. The initial resistivity of the electrolyte, which at the input was pure water at pH = 5 [*Lorne et al*., this issue], was certainly higher than this (>5000 Ωm). A higher resistivity would result in lower values of the ζ potential calculated from (14).

For Villejust quartzite data shown in Figure 10 the effective ζ potentials inferred from the streaming potentials measured for intact rocks are smaller than those calculated from the streaming potentials measured for a crushed sample for electrolyte resistivities >30 Ωm. The formation factor of Villejust quartzite is larger (Table 1) and the F/F_0 factor smaller (0.27 at 1000 Ωm) than for the Fontainebleau sandstone. Other rock samples also show smaller ζ potentials when compared with the crushed samples. For example, the ζ_{eff} potential for a crushed Vosges sandstone is measured to be −15.6 Ωm at ρ_f = 80 Ωm, while values ranging between −7 and −12 mV are measured for a rock sample containing an electrolyte with ρ_f = 385 Ωm. The range in values is caused by the uncertainty in the value of surface conductivity used for the calculation of the F/F_0 factor. In the case of the Vosges sandstone, which has a high surface conductivity of 2 ± 0.7 mS/m (Figure 7), the value of F_0 cannot be measured directly and must be inferred. Thus a small change in the value of the surface conductivity produces a large variation of the F/F_0 factor. Other rocks (AS1 and AD1) have ζ potentials smaller by a factor of 2 to 4 compared with the crushed samples.

To summarize, for electrolyte resistivities larger than ≈100 Ωm the effective ζ potentials calculated from the streaming potentials measured for intact rocks are systematically smaller than those calculated from the streaming potentials measured for crushed samples. This can be interpreted as a difference in surface state between the crushed and intact samples. However, for smaller values of the electrolyte resistivity the effective ζ potentials calculated for the rock samples are consistent with those calculated for the crushed samples. We therefore find it more plausible that the data indicate that the R_G factor is <1 and that the streaming potential is affected by a rock-dependent geometrical factor more complex than F/F_0. This factor would vary rapidly for samples near the permeability percolation threshold and hence would be quite different for crushed and intact rock samples. The data also imply that this factor is important in the domain where surface conduction becomes the dominant mechanism of electrical conduction, perhaps as a result of an interaction between the electrical double layer and the electrical flow pattern. For our hypothesis that the R_G factor is smaller than unity to be correct, we require the true ζ potential in the rock to be equal to the ζ potential in the crushed sample. Because the results using rock samples and crushed samples agree for electrolyte resistivities smaller than about 100 Ωm, crushed samples containing electrolytes with such resistivities may be used to esimtate the ζ potentials of rocks with permeabilities too small for direct streaming potential measurements.

4.2. Comparison With Crushed Samples and Effect of Permeability

The effective ζ potentials for Fontainebleau sandstone are presented as a function of permeability in Figure 11. They are compared with measurements obtained for crushed samples [*Lorne et al*., this issue]. The values measured for intact rock samples are systematically lower than the values obtained for crushed samples. No clear dependence as a function of permeability appears for the crushed or intact rock samples. However, the scatter of the data points may mask a permeability dependence of the effective ζ potential, and hence of the R_G factor. In order to study the possible permeability dependence of the effective ζ potential we studied samples during compaction. The results of such compaction experiments are presented in section 5.

5. Experimental Results During Deformation and Discussion

5.1. Compaction

Five samples were studied during compaction: FS1, FS2, FS5, FS6, and VQ1 (Table 2). Each was hydrostatically compacted by increasing the confining pressure from 0.2 MPa to a maximum value varying between 3 and 10 MPa (Table 2). We observe a reduction of the permeability by a factor of 4 to 7 for the Fontainebleau sandstone samples and a factor of 2 for the Villejust quartzite sample. *David et al*. [1994] parametrized the permeability as $k \approx \exp(-\gamma P_{\text{eff}})$, where P_{eff} is the effective

Table 2. Characteristics of the Rock Samples Used During Compaction

Sample	Maximum Confining Pressure (0.1 MPa)	Permeability, mdarcy	Formation Factor	Porosity, %
FS1	80	340–53	21.3–22.7	17.5–15
FS2	100	33–6	49–64	17–10
FS5	30	83–23.5	38–50	
FS6	30	135–70	18.9–20.2	
VQ1	100	10–4.5	223–290	7–3.4

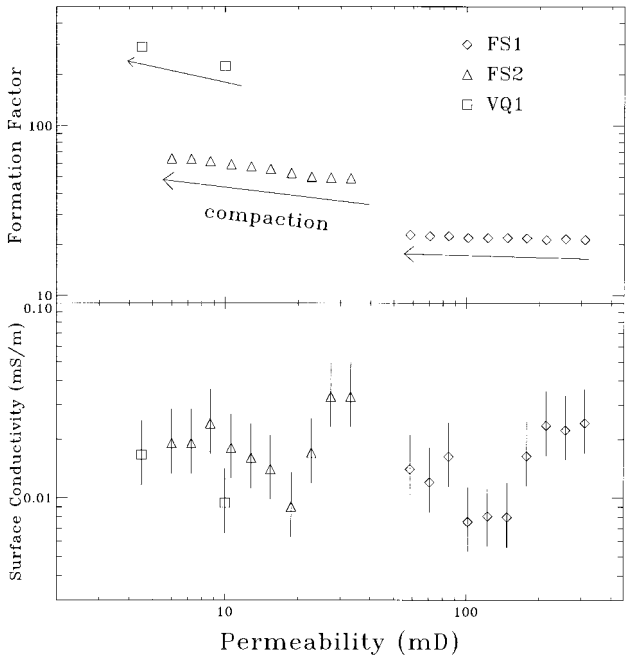

Figure 12. Bulk formation factor and surface conductivity as a function of permeability for three rock samples during compaction. The experimental error on the values of the formation factors is indicated by the size of the symbols.

pressure. The γ parameter calculated for Fontainebleau sandstone (Table 2) varies from 17 to 42 $\times$ 10^{-3}/0.1 MPa and is larger than the value of 9.8 $\times$ 10^{-3}/0.1 MPa reported by *David et al*. [1994], indicating that our samples are rather poorly cemented. Our γ parameter values are comparable with the values reported by *David et al*. [1994] for other sandstones. The γ parameter for the Villejust quartzite sample VQ1 is 8 $\times$ 10^{-3}/0.1 MPa and indicates a difference in mechanical behavior of the quartzite compared with sandstone during compaction.

At each step during the compaction of a sample the formation factor and the streaming potential were determined. For samples FS5 and FS6 the measurements were made at a fixed electrolyte resistivity of 30 and 200 Ωm, respectively. To calculate the rock sample resistivity from the measurement of its resistance, we assumed that the length and cross section of the sample remain constant during compaction. The small variation of the rock sample resistivity due to the change of length and cross section was therefore not taken into account, as the change of length and cross section of the rock samples was not monitored during our experiments. Note, however, that the main purpose of the measurement of the resistance is the calculation of the ratio F/F_0 through (13). For this ratio, and consequently for the determination of ζ_{eff}, the length and cross section of the sample are irrelevant.

For samples FS1, FS2, and VQ1 the following procedure was used. At each step in confining pressure, the KCl electrolyte solution was changed from 10 to 1000, 600, 300, 150, 60, and 30 Ωm and back to 10 Ωm. The confining pressure was then increased with the 10 Ωm electrolyte in the sample. The bulk formation factor and the surface conductivity were determined using (1) and are shown in Figure 12 as a function of permeability. The formation factor increases slightly during compaction, while the surface conductivity remains stable within experimental errors.

The evolution of the formation factor, porosity, and permeability during compaction may be parametrized, in a manner similar to that of *Bernabé* [1991], as $F \approx k^p$, $\Phi \approx k^q$, and $F \approx \Phi^m$ with $m = p/q$. The data for the formation factor in Figure 12 are well represented by such a simple parametrization. The values calculated are given in Table 3. The q parameter is the inverse of the a parameter of *David et al*. [1994], who measured $a \approx 20$ ($q \approx 0.05$) for Fontainebleau sandstone. Our results for FS1 are compatible with those of *David et al*., [1994], but the other samples have larger q. The p parameter corresponds to $-1/r$, where the r parameter is defined by *Bernabé* [1991]. For crystalline rocks a value of -0.5 for the p parameter ($r = 2$) is reported by *Bernabé* [1995]. Our values for Fontainebleau sandstone are significantly smaller, $p = -0.04$ for FS1 and $p = -0.18$ for FS2 (Table 2). The value of $p = -0.33$ for quartzite, however, is similar to the value $p = -0.5$ quoted by *Bernabé* [1995].

The surface conductivity may be similarly parametrized as $\sigma_s \approx k^\delta$. The Kozeny-Carman model (see equation (16)) predicts $\delta = -(1 + 3p)/2$. This relationship is compatible with the two data points for Villejust quartzite in Figure 12 and Table 3. For Fontainebleau sandstone the surface conductivity remains constant within experimental error during compaction, although (16) predicts that there should be an increase.

The streaming potential coefficients measured during compaction for each electrolyte resistivity are shown in Figure 13 for FS1 and FS2 and Figure 14 for VQ1. The streaming potential coefficients for each electrolyte resistivity are continuous as a function of permeability, which illustrates the reproducibility of the measurements. The streaming potential decreases significantly by a factor of 2–10 as the permeability decreases during compaction. The ratio F/F_0 is measured simultaneously and shown as a function of permeability in Figure 15 for FS1 and FS2 and in Figure 16 for VQ1. The ratio decreases by a maximum of 10–20% during compaction for FS1 and FS2 (Figure 15) and is constant during compaction for VQ1 (Figure 16). A change in the ratio F/F_0 to explain the change in the streaming potential coefficient may therefore be

Table 3. Power Law Coefficients Determined for the Rock Samples During Compaction

Sample	γ, 10^{-3}/0.1 MPa	p	q	m	δ	$-(1+3p)/2$	t_{meas}	T_{crack}	t_{tube}	t_{collapse}
FS1	23	−0.04	0.08	−0.5	0.4	−0.4	0.73	0.42	0.44	0.96
FS2	17	−0.18	0.3	−0.6	0.15	−0.2	0.89	0.17	0.29	0.81
FS5	42						0.20			
FS6	22						0.31			
VQ1	8	−0.33	0.9	−0.4	−0.7	0.005	0.61	−0.28	0.03	0.67

The measured t parameters for FS1, FS2, and VQ1 are the values averaged over the various fluid resistivities. The meanings of the p, q, m, and t parameters are given in the text.

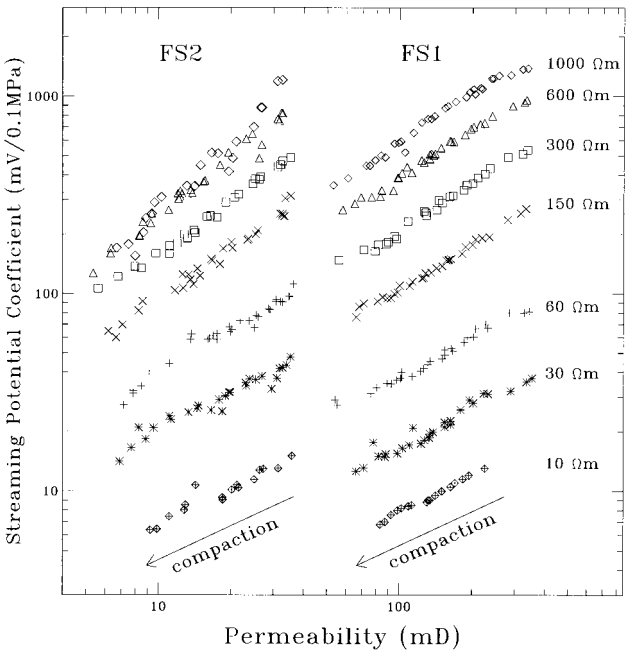

Figure 13. Streaming potential coefficient as a function of permeability for various electrolyte resistivities during compaction for Fontainebleau sandstone samples FS1 and FS2. The experimental errors are given by the size of the symbols.

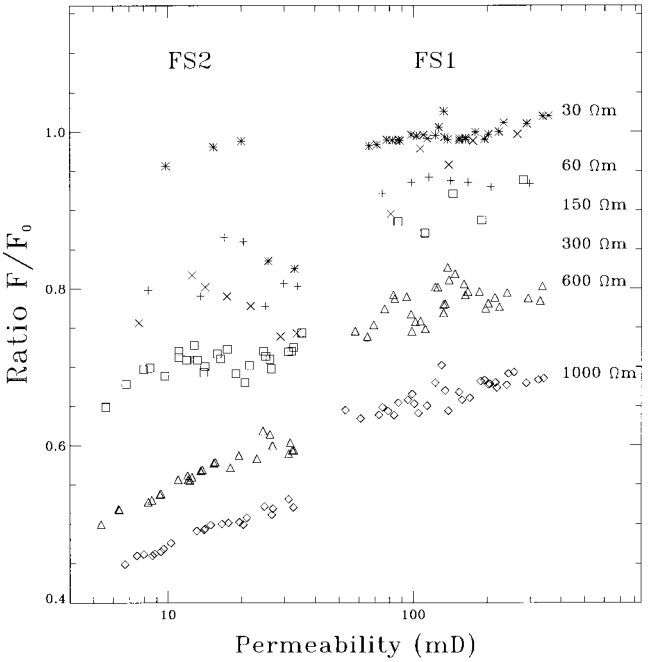

Figure 15. The ratio F/F_0, determined using equation (10), as a function of permeability for various electrolyte resistivities during compaction for Fontainebleau sandstone samples FS1 and FS2.

excluded. The fact that the reduction of streaming potential coefficient during compaction is also observed for the smaller values of the electrolyte resistivity also indicates that this variation is not due to the contribution of surface conductivity, which is important only for a resistive electrolyte ($\rho_f > 600$ Ωm, equation (1) and Figure 8).

5.2. Discussion of the Observations During Compaction

These data support our hypothesis that the streaming potential coefficient not only depends on the ζ potential but is also sensitive to the rock structure. Since the measured change of the F/F_0 factor is of the order of 10% only (whereas changes by a factor of 2–10 would be needed to account for the change

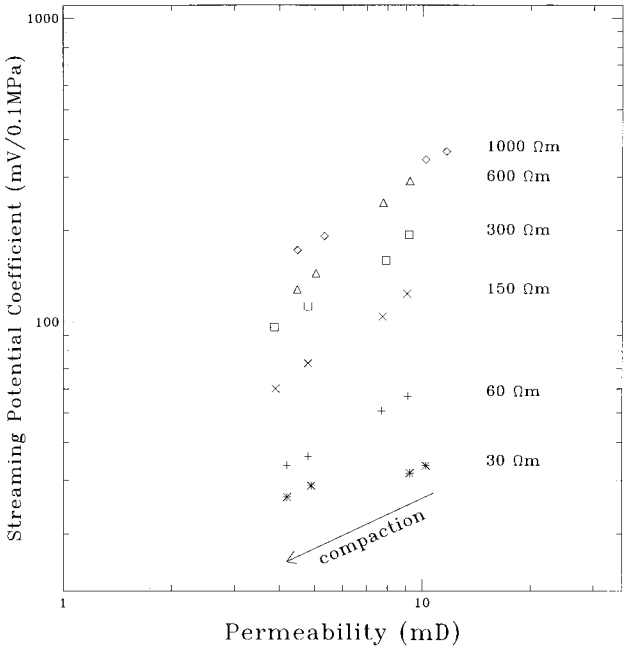

Figure 14. Streaming potential coefficient as a function of permeability for various electrolyte resistivities during compaction for Villejust quartzite sample VQ1. The experimental errors given by the size of the symbols.

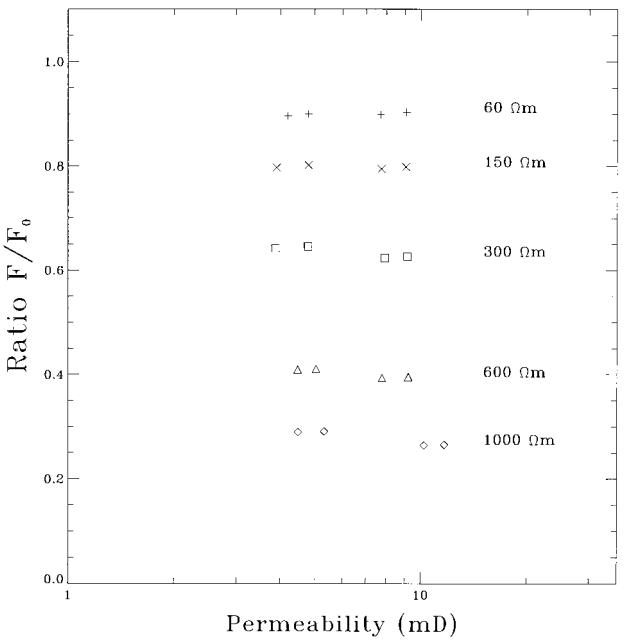

Figure 16. The ratio F/F_0, determined using equation (10), as a function of permeability for various electrolyte resistivities during compaction for Villejust quartzite sample VQ1.

in C_s), the reduction of C_s must arise from a reduction the R_G factor. During compaction, electrical and hydraulic networks are affected differently. The data indicate that the hydraulic network is evolving faster than the electrical network during compaction.

The streaming potential coefficient during compaction is parametrized as C_s or $\zeta_{\text{eff}} \approx k^t$. The values for the t parameter are shown in Figure 17 as a function of electrolyte resistivity. As evident from the data in Figures 13 and 14, the t parameter increases with increasing electrolyte resistivity. This is true for a single sample (FS1, FS2, and VQ1) and for samples FS5 and FS6 as well.

Let us assume that the physics behind the R_G factor can be parametrized using the hydraulic and electrical tortuosities defined in (10). This leads us to identify the variations of C_s during compaction with the variations of τ_e/τ_h. Then, some scaling law can be derived for the t parameter as a function of the other scaling parameters p and q. As another equation is needed for the porosity, we use

$$\Phi = \tau_e m^g, \tag{17}$$

where g is a geometrical exponent equal to 1 for cracks and 2 for tubes, from dimensional arguments following *Bernabé* [1991]. The electrical tortuosity is added in order to account for the electrical efficiency of pore space [*Herrick and Kennedy*, 1994]. Equation (17) implies that the channels open to hydraulic flow have a small contribution to the porosity, in contrast to the channels which are electrically connected.

The system of (10), (11), and (17) is then redundant [*Bernabé*, 1991], and the t parameter can be calculated

$$t = \frac{1}{2} + \frac{p}{2} - \frac{q-p}{2q}. \tag{18}$$

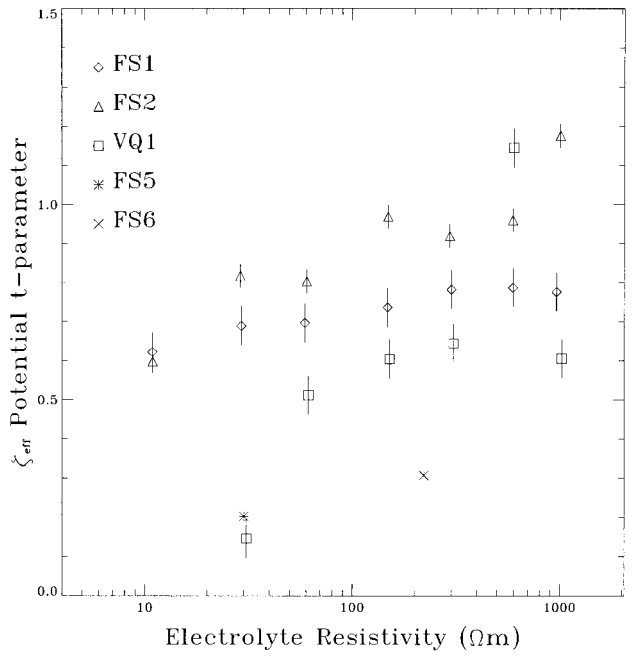

Figure 17. The permeability exponent t parameter of the effective ζ potential versus electrolyte resistivity during compaction ($\zeta_{\text{eff}} \sim k^t$) for Fontainebleau sandstone and Villejust quartzite samples.

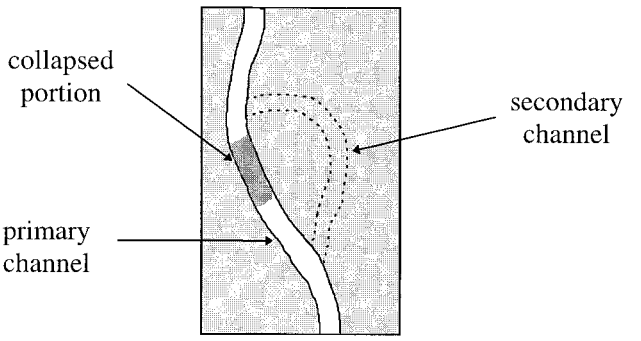

Figure 18. A simple model for the evolution of transport properties associated with pore collapse during compaction. When the shaded portion collapses, fluid percolation proceeds through a secondary path.

This prediction is compared with the measurements in Table 3 separately for cracks and tubes, inserting the measured values for p and q in (18) to obtain a prediction for t. The calculated values are much smaller than the measured values for FS1, FS2, and VQ1 but are comparable with the results for FS5 and FS6. This indicates that this simple modified equivalent channel model does not capture all the essential physical features of the data.

This model also does not account for the observed variation of the t parameter with electrolyte resistivity (Figure 17). The role of the electrolyte is important: the t parameters for FS1, FS2, and VQ1 are larger than for FS5 and FS6. This fact may be due to the experimental procedure. As described before, the compaction of FS1, FS2, and VQ1 was done for $\rho_f = 10$ Ωm. Some conductive electrolyte may have been trapped in the sample during the compaction, and the increase of the t parameter with increasing electrolyte resistivity would then be related to the resistivity contrast between the flowing and trapped electrolyte.

Collapse of pores [*Zhang et al*., 1990] would also produce an enhancement of the t parameter. A simple mechanism for the evolution due to pore collapse is illustrated in Figure 18. In this model it is assumed that the evolution of the transport property is dominated by the length of the percolating paths, with little change in pore throat size. During compaction, some parts of the percolation path collapse, and flow proceeds through a more complex path. The evolution of the permeability is thus due to the evolution of the tortuosity. The convection current would scale like the permeability as $1/\tau_h$, the resistance like the inverse of the formation factor, and therefore the streaming potential, which combines (5) and (6), like

$$t_{\text{collapse}} = 1 + p. \tag{19}$$

The values of the t parameter predicted by this model are close to 1 and in good agreement with the measured values (Table 3) for FS1, FS2, and VQ1. Thus, if channels with pore collapse have a significant contribution to the formation factor, which would be the case if this collapse occurs with a conductive electrolyte, then the value of the t parameter is increased.

Thus the observed reduction of the streaming potential coefficient during compaction suggests an important effect of coupled percolation networks contributing to electrical and hydraulic flows. It can be interpreted as evidence that the hydraulic tortuosity is increasing faster than the electrical tortuosity during compaction. Using the simple models presented

Table 4. Characteristics of the Rock Samples Used for the Rupture Experiments

Sample	Confining Pressure, MPa	Failure Stress, MPa	Electrolyte Resistivity, Ωm	Relative C_s Reduction During Compression, %	Stress of Minimum C_s (Fraction of Failure Stress), %	Relative C_s Variation Before Rupture, %	Stress of Maximum C_s (Fraction of Failure Stress), %
FS4	3	62	500	25	79	27	NO
FS5	3	99	200	12	79	30	80
FS6	1	74	200	30	73	34	88
VQ2	1.5	98	200	48	65	50	NO
VQ3	0.75	134	100	78	NO	NO	NO

NO, not observed.

above, pore collapse could explain the sensitivity of the t parameter to electrolyte resistivity, and it might thus be the dominating compaction mode in our experiments.

5.3. Uniaxial Compression and Rupture

Five samples (FS4, FS5, FS6, VQ2, and VQ3) were subject to uniaxial compression and rupture (Tables 1 and 4). A moderate confining pressure of 0.75 to 3 MPa (indicated in Table 4) was applied and kept constant while the uniaxial force was increased slowly, at rates varying between 2×10^{-7} and 8×10^{-7} s^{-1}, up to failure. The yield failure stress varies from 62 to 99 MPa for Fontainebleau sandstone samples and was 134 MPa for VQ3 (Table 4). These values are significantly smaller than for the samples used by *Jouniaux and Pozzi* [1995b], for which an average yield stress of 250 MPa was reported at confining pressures up to 10 MPa. For sample FS4, electrolyte circulation was still possible in the sample, and electrical measurements could be performed after failure (point 17 in Figure 19). For the four other samples the rock failure resulted in serious damage to the electrode and sample assembly, and no meaningful postfailure measurements were possible. During these experiments the samples were saturated with an electrolyte of moderate resistivity, varying between 100 and 500 Ωm (Table 4). These values were chosen in order to establish a significant streaming potential while keeping the contribution of surface conductivity negligible compared with the bulk conductivity.

The streaming potential coefficient and the formation factor are shown as a function of permeability in Figure 19 for the three Fontainebleau sandstone samples FS4, FS5, and FS6 and in Figure 20 for the two Villejust quartzite samples VQ2 and VQ3. The variation of the permeability and the formation factor are different from sample to sample, but common features emerge from the behavior of the streaming potential coefficient.

For FS4, FS6, VQ2, and VQ3 the uniaxial compression first produces a phase of decreasing streaming potential coefficient of the same order of magnitude as the one observed during compaction. The magnitude of this reduction varies from 12 to 30% for Fontainebleau sandstone and from 48 to 78% for Villejust quartzite. The mechanism for this decrease of C_s is hypothesized to be of the same nature as the mechanism producing the decrease associated with compaction and therefore suggests that the hydraulic tortuosity increases faster than the electrical tortuosity during compression. A decrease of streaming potential during uniaxial compression in the quasi-elastic domain was also observed by *Jouniaux and Pozzi* [1995b] for one Fontainebleau sandstone sample but not for two other samples. This initial phase is also associated with an increase of the formation factor (except for sample VQ3, for which no increase of formation factor is observed), compatible with the closure or collapse of cracks.

After the initial phase of streaming potential coefficient decrease, a secondary increase is observed for all our Fontainebleau sandstone samples (Figure 19) and one of the two Villejust quartzite samples (Figure 20). The minimum of the streaming potential occurs at 73% and 79% of the failure stress for Fontainebleau sandstone (Table 4), a value remarkably constant from sample to sample, despite the large differences in the yield stress. Our measurements therefore confirm the earlier observation of this phenomenon by *Jouniaux and Pozzi* [1995b], who measured that the minimum in C_s occurs at a fraction of the failure stress varying between 72 and 86%. This indicates that the increase in the streaming potential coefficient reflects some generic property of the rock, rather than the details of the percolation networks. For samples FS4, FS6, and VQ2 the minimum of C_s corresponds to the maximum of the formation factor (Figures 19 and 20), which may indicate that this increase in C_s corresponds to the onset of dilatancy, which is possibly associated with an increase of permeability. However, the onset of dilatancy is usually observed to occur at 40–50% of the failure stress [*Jouniaux et al*., 1992; *Glover et al*., 1996, 1997b].

For samples FS5 and FS6 the increase of streaming potential coefficient is followed by a decrease before failure (Figure 19), as was also reported by *Jouniaux and Pozzi* [1995b] for two of three samples. The maximum in C_s occurs at 80% and 88% of the yield stress (Table 4). The overall variation of the streaming potential coefficient from initial state up to rupture (Table 4) is ~30% for Fontainebleau sandstone and ~50% for VQ1.

The variations of streaming potential coefficient before rupture are not always associated with clear changes of permeability, as also noted by *Jouniaux and Pozzi* [1995b], but are systematically associated with changes of the formation factor. This indicates that the streaming potential must vary due to changes in the pattern of the conduction current. The hydraulic flow pattern and the electric flow pattern may evolve differently before rupture, although they are sometimes strongly correlated, for example, during compaction and the initial phase of uniaxial compression. A decoupling occurs after the onset of dilatancy, producing both increases (FS4, VQ2) and decreases (FS6) of the streaming potential coefficient.

5.4. Discussion of the Fracture Experiments

This behavior of the streaming potential coefficient can be attributed to changes in the surface properties and hence the ζ potential during deformation or to changes in the relationship between hydraulic and electrical flow patterns, as discussed

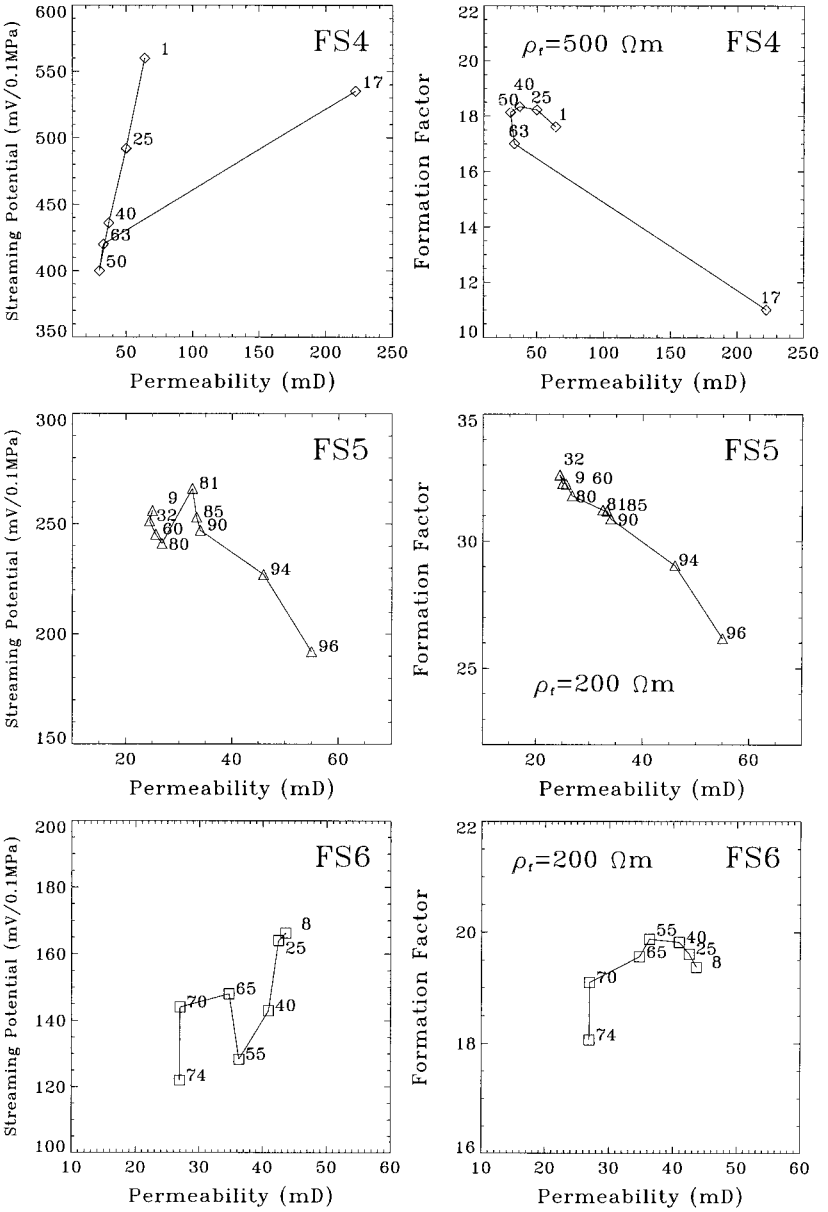

Figure 19. Streaming potential coefficient and formation factor during uniaxial compression and rupture for three Fontainebleau sandstone samples. The number indicated near each data point corresponds to the value of the uniaxial force. The values of the electrolyte resistivity were 500 Ωm for FS4 and 200 Ωm for FS5 and FS6.

before. Changes in the surface properties might be expected before rupture, when new cracks are opened. However, these are not likely to occur during the initial uniaxial compression phase when preexisting cracks are closing, during which the largest variations of the streaming potential coefficient are observed. It is therefore considered likely that the dominating factor affecting the streaming potential during deformation is, again, the geometrical R_G factor.

Qualitatively, variations of the streaming potential coefficient can be related to variations of the R_G factor in the simple model illustrated in Figure 21. Let us imagine that the hydraulic flow is controlled by some typical channel (Figure 21a), while the electrical flow would be controlled by a dense network of cracks, of different shape and aspect ratio, and also filled with fluid. Since the cracks are more numerous, the percolation paths are less complex for electrical current, and the corresponding electrical tortuosity is smaller than the hydraulic tortuosity, as observed in our experiments ($R_G < 1$). During compaction (Figure 21b), or uniaxial compression, the electrical network is not affected, while the hydraulic flow becomes more and more complicated. This phase would naturally lead to a decrease of the streaming potential. When the onset of dilatancy occurs (Figure 21c), the cracks open, possibly connecting several of these cracks to the flow channel. In this simple model the hydraulic flow itself is not affected directly by this onset of dilatancy, but the complexity of the electrical connectivity is increased, and therefore the corresponding tortuosity increased, although the net formation fac-

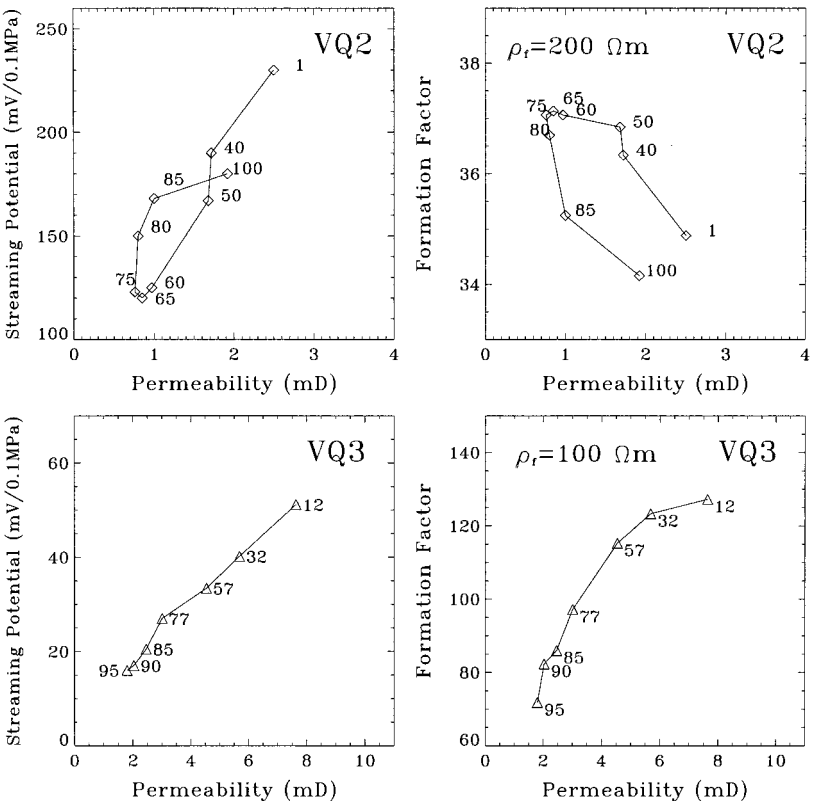

Figure 20. Streaming potential coefficient and formation factor during uniaxial compression and rupture for two Villejust quartzite samples. The number indicated near each data point corresponds to the value of the uniaxial force. The values of the electrolyte resistivity were 200 Ωm for VQ2 and 100 Ωm for VQ3.

tor is decreasing because the cracks are wider. At some point (Figure 21d) the cracks might be wide enough to compete with the flow channel, increasing the complexity of the flow channel and hence the hydraulic tortuosity. During that final phase, both the electrical and hydraulic tortuosities increase, and the net effect on the streaming potential might be an increase or a decrease depending on which of the competing effects dominates.

Some part of the variation of the streaming potential may be due to a change in the electrolyte resistivity or composition. For sample FS6 the electrolyte was sampled and analyzed by electrophoresis after flowing through the cell for each step of the applied force. The results are presented in Figure 22, together with the measured resistivity. The electrolyte resistivity decreased during the initial phase of the uniaxial compression by ~10%, which would induce a decrease in the streaming potential coefficient of the same amount, according to (7), since the sensitivity of the ζ potential to electrolyte resistivity is small [*Pride and Morgan*, 1991; *Revil and Glover*, 1997; *Lorne et al*., this issue]. However, the observed decrease in C_s was 30% for this sample, so the bulk of the change of the streaming potential coefficient is probably not due solely to the evolution of the electrolyte chemistry inside the sample. Trace amounts of ions like Al^{3+} can have a large effect on the ζ potential [*Ishido and Mizutani*, 1981; *Morgan et al*., 1989], but such effects are not likely for the magnitude of the electrolyte resistivity used in our experiments [*Lorne et al*., this issue]. No increase of electrolyte resistivity is associated with the subsequent increase of streaming potential coefficient.

The concentrations of K^+ and Cl^- ions were relatively constant during the experiment. However, a significant increase in the concentration of SO_4^{2-} ions is observed at 75% of the rupture strength. This observation supports the fact that the point of minimum streaming potential is associated with the opening of new fractures and the onset of dilatancy. Sulfate ions are probably released by reactions occurring in the cement between quartz grains. The increase in concentration of sulfate ions would produce a reduction of the ζ potential [*Morgan et al*., 1989; *Lorne et al*., this issue], but this concentration is too small to have an observable effect. It would certainly not explain the enhancement of streaming potential coefficient, which we rather postulate to arise from the changes in electrical and hydraulic percolation patterns.

The observation of a release of sulfate ions in sandstone before failure is, however, interesting in itself, because an increase in the concentration of sulfate ions of 30% was observed in the groundwater before the Kobe earthquake [*Tsunogai and Wakita*, 1995], associated with an increase of 10% of the concentration of chloride ions. Our observation supports the hypothesis that the increase of sulfate ions reflects a change in the deformation regime of the rocks and might be a useful indicator of deformation and rupture at crustal scales.

6. Conclusions and Implications for Earthquake Precursors

In this paper, streaming potential coefficients in rock samples have been measured during deformation and rupture and compared with streaming potential coefficients obtained using crushed samples. The results show that the streaming potential

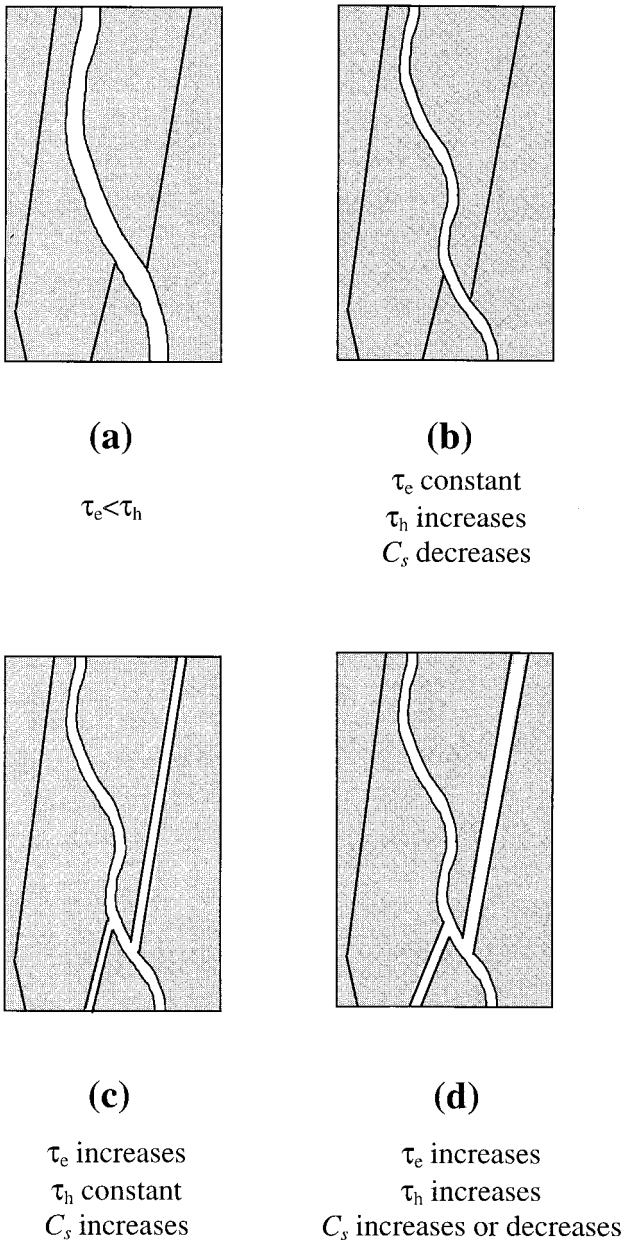

Figure 21. A simple conceptual model for the evolution of the tortuosities and the streaming potential coefficients during uniaxial compression: (a) initial state with a main channel for hydraulic flow and a network of smaller channels for electrical current, (b) initial phase of uniaxial compression; the typical pore radius is reduced and percolation paths get longer, (c) onset of dilatancy: cracks open, and (d) cracks are large enough to compete with the main flow channel for the hydraulic flow.

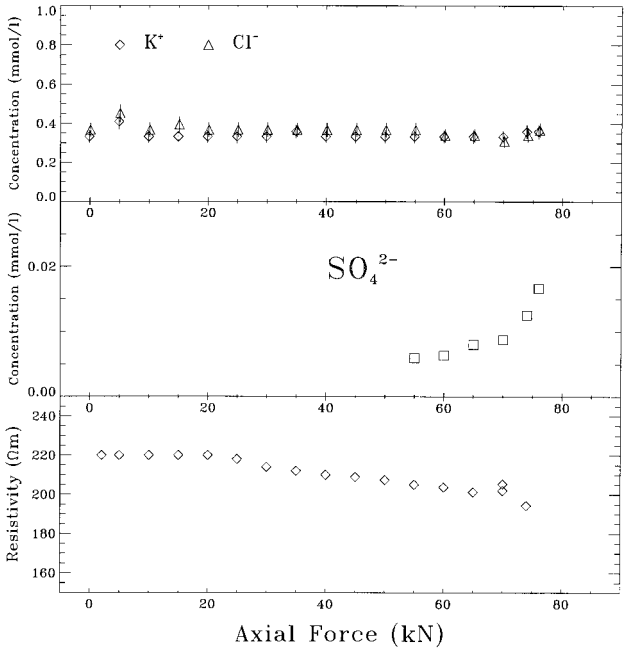

Figure 22. Concentrations of K^+, Cl^-, and SO_4^{2-} ions and the electrolyte resistivity (coming out of the sample, see Figure 3) during rupture of Fontainebleau sandstone sample FS6, as a function of the uniaxial force. The ion concentrations are measured by capillary electrophoresis and have an uncertainty of 10%.

coefficient is sensitive to the pattern of percolation in the rock, in contrast with the predictions from simple capillary models. Our results show that the streaming potential is reduced significantly during compaction or uniaxial compression. Although the order of magnitude of the effect and its sensitivity to the resistivity of the electrolyte used point to the importance of pore collapse in the deformation of Fontainebleau sandstone, a detailed numerical modeling of the results remains to be done. Network calculations could be of great help in understanding the details of the rock physics involved and the exact role of the percolation patterns [*David*, 1993; *Bernabé*, 1995, 1998]. Streaming potentials therefore appear to be a powerful tool, complementary to standard transport properties (permeability and resistivity), for elucidating the physical processes in rocks. An important question in rock physics which could be addressed using streaming potential measurements is the effect on the transport properties of the coupling between two types of percolation networks, i.e., cracks and tubes. This problem was studied using sintered porous media [*Mattisson et al.*, 1997], and it was shown that the effective transport properties are not the sum of the contributions of each network separately. Measuring the streaming potential of such sintered media could be of great value.

A consistent increase of the streaming potential coefficient was observed after the onset of dilatancy, in agreement with earlier results [*Jouniaux and Pozzi*, 1995b]. These observations support the use of EKE as a physical basis for earthquake precursors [*Mizutani et al.*, 1976].

If we imagine a rock volume through which a stationary permanent flow is maintained by some reservoir at depth and if this source is located in the nucleation zone of an earthquake, then the spontaneous potential observed at the surface would show a strong modulation before failure, similar to our observations in the laboratory: a slowly varying decrease of the anomaly with time, followed by an increase after the dilatant phase is reached and, possibly, a fast decrease before failure. To observe such a signal, it would be necessary to be close to the epicenter, as the measured signal attenuates quickly with distance away from the electrical source [*Bernard*, 1992]. Such a mechanism does not necessarily imply a strong coseismic potential variation [*Bernard*, 1992]. The final state of the po-

tential generating zone may be a compressive state, or may be equivalent to the fracturing of sample FS4, for which the final state produced a streaming potential similar to the initial state (Figure 19). Such potential variations would only be observed at locations where groundwater flow maintains a strong static electrical source.

Acknowledgments. The authors are grateful to the Laboratoire de Détection et de Géophysique for financial and technical support. Funds were also received from the French Ministry of Environment. Most of the experiments were performed with the help of Thierry Froidefond and Pierre Lalance. In addition, Jean Aupiais and Denise Fresquet helped with advises, equipment, measurements, and analysis of the electrolytes. Patrick Dupont is thanked for the fabrication of many pieces of the apparatus. The authors thank Laurence Jouniaux and Jean-Pierre Pozzi for initial guidance. Fruitful discussions with Steve Pride, Michel Darot, André Revil, and Yves Bernabé are acknowledged during the early stages of the experiments. Laurence Jouniaux, Steve Pride, and Paul Glover are thanked for their inspiring suggestions on an early draft. Last but not least, M. Johnston and B. J. Wanamaker are thanked for their extremely detailed and constructive review.

References

Bernabé, Y., Pore geometry and pressure dependence of the transport properties in sandstones, *Geophysics*, *56*, 436–446, 1991.

Bernabé, Y., The transport properties of networks of cracks and pores, *J. Geophys. Res*., *100*, 4231–4241, 1995.

Bernabé, Y., Streaming potential in heterogeneous networks, *J. Geophys. Res*., *103*, 20,827–20,842, 1998.

Bernard, P. Plausibility of long distance electrotelluric precursors to earthquakes, *J. Geophys. Res*., *97*, 17531–17546, 1992.

Bikerman, J. J., Electrokinetic potentials, in *The Encyclopedia of Electrochemistry*, edited by C. A. Hampel, pp. 471–475, Reinhold, New York, 1964.

Brown, S. R., Fluid flow through rock joints: The effect of surface roughness, *J. Geophys. Res*., *92*, 1337–1347, 1987.

Brown, S. R., Transport of fluid and electric current through a single fracture, *J. Geophys. Res*., *94*, 9429–9438, 1989.

David, C., Geometry of flow paths for fluid transport in rocks, *J. Geophys. Res*., *98*, 12,267–12,278, 1993.

David, C., T.-f. Wong, W. Zhu, and J. Zhang, Laboratory measurement of compaction-induced permeability change in porous rocks: Implications for the generation and maintenance of pore pressure excess in the crust, *Pure Appl. Geophys*., *143*, 425–456, 1994.

Davis, J. A., R. O. James, and J. O. Leckie, Surface ionization and complexation at the oxide/water interface, *J. Colloid Interface Sci*., *63*, 480–499, 1978.

Duplessis, J. P., and L. I. Roos, Predicting the hydrodynamic permeability of sandstone with a pore scale model, *J. Geophys. Res*., *99*, 19,771–19,776, 1994.

Glover, P. W. J., P. G. Meredith, P. R. Sammonds, and S. A. F. Murrell, Ionic surface conductivity in sandstone, *J. Geophys. Res*., *99*, 21,635–21,650, 1994.

Glover, P. W. J., J. B. Gomez, P. G. Meredith, S. A. Boon, P. R. Sammonds, and S. A. F. Murrell, Modelling the stress-strain behaviour of saturated rocks undergoing triaxial deformation using complex electrical conductivity measurements, *Surv. Geophys*., *17*, 307–330, 1996.

Glover, P. W. J., K. Matsuki, R. Hikima, and K. Hayashi, Fluid flow in fractally rough synthetic fractures, *Geophys. Res. Lett*., *24*, 1803–1806, 1997a.

Glover, P. W. J., J. B. Gomez, P. G. Meredith, K. Hayashi, P. R. Sammonds, and S. A. F. Murrell, Damage of saturated rocks undergoing triaxial deformation using complex electrical conductivity measurements: experimental results, *Phys. Chem. Earth*, *22*, 57–61, 1997b.

Herrick, D. C., and W. D. Kennedy, Electrical efficiency—A pore geometry theory for Interpreting the electrical properties of reservoir rocks, *Geophysics*, *59*, 918–927, 1994.

Ishido, T. and H. Mizutani, Experimental and theoretical basis of electrokinetic phenomena in rock-water systems and its applications to geophysics, *J. Geophys. Res*., *86*, 1763–1775, 1981.

Jouniaux, L., and J. P. Pozzi, Permeability dependence of streaming potential in rocks for various fluid conductivities, *Geophys. Res. Lett*., *22*, 485–488, 1995a.

Jouniaux, L., and J. P. Pozzi, Streaming potential and permeability of saturated sandstones under triaxial stress: Consequences for electrotelluric anomalies prior to earthquakes, *J. Geophys. Res*., *100*, 10,197–10,209, 1995b.

Jouniaux, L., and J. P. Pozzi, Laboratory measurements anomalous 0.1–0.5 Hz streaming potential under geochemical changes: Implications for electrotelluric precursors to earthquakes, *J. Geophys. Res*., *102*, 15,335–15,343, 1997.

Jouniaux, L., J. P. Pozzi, M. Brochot, and C. Philippe, Resistivity changes induced by triaxial compression in saturated sandstones from Fontainebleau (France), *C. R. Acad. Sci., Ser. II*, *315*, 1493–1499, 1992.

Knackstedt, M. A., and J. P. Duplessis, Simple permeability model for natural granular media, *Geophys. Res. Lett*., *23*, 1609–1612, 1996.

Lockner, D. A., and J. D. Byerlee, Complex resistivity measurements of confined rocks, *J. Geophys. Res*., *90*, 7837–7847, 1985.

Lorne, B., F. Perrier, and J. P. Avouac, Streaming potential measurements, 1, Properties of the electrical double layer from crushed rock samples, *J. Geophys. Res*., this issue.

Mattisson, C., M. A. Knackstedt, and T. S. Senden, Transport in fractured porous, *Geophys. Res. Lett*., *24*, 495–498, 1997.

Mizutani, H., T. Ishido, T. Yokokura, and S. Ohnishi, Electrokinetic phenomena associated with earthquakes, *Geophys. Res. Lett*., *3*, 365–368, 1976.

Morgan, F. D., E. R. Williams, and T. R. Madden, Streaming potential properties of Westerly granite with applications, *J. Geophys. Res*., *94*, 12,449–12,461, 1989.

Ogilvy, A. A., M. A. Ayed, and V. A. Bogoslovsky, Geophysical studies of water leakages from reservoirs, *Geophys. Prospect*., *17*, 36–62, 1969.

Overbeek, J. T., *Colloid Science*, edited by H. R. Kruyt, Elsevier, New York, 1960.

Perrier, F., M. Trique, B. Lorne, J. P. Avouac, S. Hautot, and P. Tarits, Electric potential variations associated with lake level variations, *Geophys. Res. Lett*., *25*, 1955–1958, 1998.

Pride, S., Governing equations for the coupled electromagnetics and acoustics of porous media, *Phys. Rev. B Condens. Matter*, *50*, 15,678–15,696, 1994.

Pride, S. R., and F. D. Morgan, Electrokinetic dissipation induced by seismic waves, *Geophysics*, *56*, 914–925, 1991.

Revil, A., and P. W. J. Glover, Theory of ionic-surface electrical conduction in porous media, *Phys. Rev. B Condens. Matter*, *55*, 1757–1773, 1997.

Revil, A., M. Darot, and P. A. Pezard, From surface electrical properties to spontaneous potentials in porous media, *Surv. Geophys*., *17*, 331–360, 1996.

Ruffet, C., Y. Gueguen, and M. Darot, Complex conductivity measurements and fractal nature of porosity, *Geophysics*, *56*, 758–768, 1991.

Scheidegger, A. E., *The Physics of Flow Through Porous Media*, 353 pp., Univ. of Toronto Press, Toronto, Ont., Canada, 1974.

Trique, M., P. Richon, F. Perrier, J. P. Avouac, and J. C. Sabroux, Radon emanation and electric potential variations associated with transient deformation in the vicinity of reservoir lakes, *Nature*, *399*, 137–141, 1999.

Tsunogai, U., and H. Wakita, Precursory chemical changes in ground water: Kobe earthquake, Japan, *Science*, *269*, 61–63, 1995.

Walsch, J. B., S. R. Brown, and W. B. Durham, Effective media theory with spatial correlation for flow in a fracture, *J. Geophys. Res*., *102*, 22,587–22,594, 1997.

Zhang, J., T.-f. Wong, and D. M. Davis, Micromechanics of pressure-induced grain crushing in porous rocks, *J. Geophys. Res*., *95*, 341–352, 1990.

J.-P. Avouac, B. Lorne, and F. Perrier, Commissariat a l'Energie Atomique, Laboratoire de Detection et de Geophysique, BP12, F-91680 Bruyeres-le-Chatel, France. (perrier@ldg.bruyeres.cea.fr).

(Received April 3, 1998; revised March 26, 1999;
accepted April 20, 1999.)